www.czasopisma.pan.pl PAN POLSKA AKADEMIA NAUK www.journals.pan.pl

Archives of Acoustics Vol. **48**, No. 3, pp. 425–432 (2023), doi: 10.24425/aoa.2023.145241

Research Paper

PZT Asymmetrical Shape Optimization in Active Vibration Reduction of Triangular Plates

Adam BRAŃSKI, Romuald KURAS*

Department of Electrical and Computer Engineering Fundamentals
Rzeszow University of Technology
Rzeszow, Poland

*Corresponding Author e-mail: r.kuras@prz.edu.pl

(*received November 18, 2022; accepted March 11, 2023*)

The article presents the new 2D asymmetrical PZT (a-PZT) and its effectiveness in the active reduction of triangular plate vibrations. The isosceles right triangular plate with simply supported edges was chosen as the research object. To determine the a-PZT asymmetry and its distribution on the plate, a maximum bending moment criterion for the beam was used. First of all, this criterion points out exact center location of the a-PZT. It was at the point, at which the plate bending moment has reached its maximum value. Next, at this point, it was assumed that the piezoelectric consists of active fibers located radially from the center. Each fiber acted on the plate as a separate actuator. Next, at each direction, the actuator asymmetry was found mathematically by minimizing the amplitude of the vibrations. By connecting the outer edges of individual fibers, the 2D a-PZT was obtained. It was quantitatively confirmed that the effectiveness of the new a-PZT was the best compared with the effectiveness of the standard square and the circular PZTs, adding the same exciting energy to the PZTs.

Keywords: triangular plate; actuator (PZT); active vibration reduction; vibration reduction coefficient; effectiveness coefficient.

1. Introduction

Active vibration reduction is applied to many common structural elements such as: beams, plates, shells, shafts, trusses. A significant problem is to increase the efficiency of active reduction. Recent publications on this subject have focused on the problem of optimizing the location and orientation of mainly square or circular (regular) PZTs on a structure. Aridogan and Basdogan (2015) presented the review of active vibration and noise suppression of plate-like structures with PZT. This article shows numerical methods and experimental tools to study various aspects of controller architecture, i.e., the variety of control systems in active vibration control and their influence on the actuator configuration. Zhang *et al.* (2018) investigated topology optimization of the electrode coverage of a laminated rectangular plate with piezoelectric patches attached. In this case, the optimization was carried out in terms of minimizing energy consumption. Zorić *et al.* (2019) presented research on piezofiber reinforced composite actuators (PFRC) and the optimization concerning the size, orientation and location of the actuator. Gonçalves *et al.* (2017) considered active vibration reduction with embedded PZTs. Similarly to Zorić *et al.* (2019), the topology optimization method was used to find the optimum design of actuators; the aim of the optimization was to determine the distribution of piezoelectric material that maximizes controllability for a given mode shape. The shape of the PZT layer was defined using the Sequential Linear Programming algorithm. Gardonio and Casagrande (2017) published the general guidelines for dimensioning the PZT patch and electrical shunt to maximize the electro-mechanical vibration absorption. Optimization of electrode distribution for two-dimensional structures was also presented by Wang (2003) and the results of the opti-

mization algorithms used confirm the correctness of the maximum bending moment criterion (Brański, Kuras, 2022). Donoso and Sigmund (2009) considered optimization of the thickness of the PZT layers and its width profile on the beam structure. Sun *et al.* (2022) investigated analytically, numerically and experimentally the problem of active vibration control of a simply supported rectangular plate. The method was based on the plate deflection theory. In the case of homogeneous boundary conditions and regular structure (rectangular plate), this theory coincides with the theory based on the maximum bending moment criterion (Brański, Kuras, 2022). Trojanowski and Wiciak (2020) used ring-shaped sensor-actuator hybrid to investigate efficiency of such a system. The compared shapes of actuators are: square, disc, and ring with larger and smaller sensor part. Kozień and Ścisło (2015) investigated bending vibrations of the beams. The PZT was located at the maximum bending moment of the structure and the parameter for control algorithm was the actual bending moment in the previous time step.

The methods used in the cited articles are most often based on regular PZTs, optimal distribution of piezoelectric material or optimal distribution of electrodes. But the parameter that would influence on the effectiveness of active vibration reduction could be an asymmetric shape of the PZT. In the 1D case (Brański, Kuras, 2022), the geometric parameter is optimized which leads to the asymmetry of the PZT. Other parameters that can be also optimized, e.g., the PZT location, the voltage supplied to the transducer. However, for 2D structures, for example triangular, there is one more parameter that follows from the shape of the actuator and its orientation on the structure.

The aim of the paper is to find an asymmetrical shape of the PZT, i.e., a-PZT, and indicate its location on the triangular plate so that it ensures the maximum reduction of vibration. To achieve this aim, the maximum bending moment criterion is applied. Since the problem is more complex than in 1D problem, then the more complex shape and structure of the a-PZT is chosen into consideration, i.e., it consists of piezoceramic fibers. Hence, each fiber can be analyzed separately, leading to separate asymmetries of the individual fibers.

The common feature of all the fibers is that they have one common point (the basic a-PZT point), which is at the point where the plate bending moment reaches its absolute maximum. Each of the fibers can be considered separately as a one-dimensional PZT. The asymmetry of a separate fiber is determined separately and means that the forces on opposite edges have different values and the basic a-PZT point is not in the center of the fiber. Since this point is fixed, it leads to the determining different arms of forces on opposite edges of separate fibers. It should be added that the values of these forces are determined assuming that the asymmetric moments of both pairs of forces are equal at all fibers. Connecting the outer edges of separate fibers, the 2D a-PZT is obtained. Minimizing amplitude of the plate vibration, forces values of the fibers are determined. The effect of the a-PZT acting, measured by the reduction of vibration amplitude, translates into reduction of the bending moment and shear force.

At the end, the effectiveness of a-PZT and the regular actuators, namely, square PZT (s-PZT) and circular PZT (c-PZT) are compared, assuming that the energy added to all PZTs is the same.

2. Forced vibration of the triangular plate with PZT actuator

The governing equation of transverse vibration of the triangular plate is based on Kirchhoff's classical small deflection theory. In the steady state the equation takes the form (Fuller *et al.*, 1997; Hansen, Snyder, 1997):

$$c^2\Delta^2 w - \omega_f^2 w = \frac{f}{\varrho h}, \tag{1}$$

where $f = f_E + f_P$ – the external forces, $f_E = f_E(x,y)$ – the exciting force, $f_P = f_P(x,y)$ – the forces interacting between PZT and the plate, w – the transverse displacement in a steady state, ω_f – the excited frequency, $c^2 = D/(\varrho h)$, ϱ – the mass density, h – the thickness, $D = \frac{Eh^3}{12(1-\nu^2)}$ – the flexural rigidity, E – Young's modulus, ν – Poisson's ratio, Δ – the Laplace operator, $\Delta w = D_x^2 w + D_y^2 y$.

The boundary conditions for the simply supported right triangular plate are defined as follows:

$$w = 0, \qquad M_{nn} = 0, \tag{2}$$

where Eq. (2) relates to all of the edges, Fig. 1, M_{nn} – normal bending moment, n – normal to an edge.

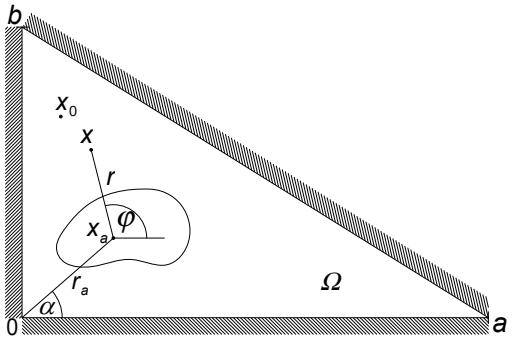

Fig. 1. Simply supported right triangular plate with global symbols: $x_a = (x_a, y_a)$; $x = (x,y) = (r_a + r) = (r_a\cos\alpha + r\cos\varphi, r_a\sin\alpha + r\sin\varphi)$.

An external excitation is in the following form:

$$f_E(x,y) = f_0\delta(x-x_0, y-y_0), \tag{3}$$

where f_0 – amplitude of the exciting force, $x_0 = (x_0, y_0)$ – point of applying the exciting force.

The active forces of the PZT interaction depend on its shape, and for square and circular shapes they can be found, for example, in (Brański, Szela, 2008; 2010). However, these interaction forces for the a-PZT are derived below.

2.1. Free vibration problem by the superposition method

The superposition method was applied to solve the free vibration problem (Gorman, 1983; 1999; Rao, 2007; Saliba, 1990; 1996). It is the solution of the homogeneous Eq. (1), i.e., $\Delta^2 w - \lambda^4 w = 0$, λ – eigenvalue, $\lambda^4 = \omega_f^2 \varrho h/D$, and simply supported boundary conditions along three edges (Leissa, 1969), Eq. (2). First of all, as in standard, non-dimensional coordinates are introduced, i.e., $\xi = x/a$, $\eta = y/b$, and ψ – the plate aspect ratio. Then, the idea of the Lévy solution, based on two building blocks BB1 and BB2, is used, Fig. 2.

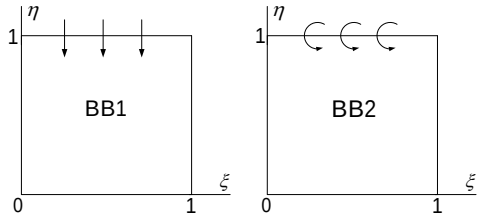

Fig. 2. Building blocks used in the solution.

The solution is assumed to be of the form satisfying SS-BC for each building block. This solution satisfies the SS-BC in advance along the edge $\xi = 0$, $\xi = 1$, and $\eta = 0$. According to the displacement and bending moments along the edge $\eta = 1$, the solution for the BB1 can be formulated as:

$$w_{\mathrm{BB1}}(\xi,\eta) = \sum_{m}^{m^*} G_{1m}\theta_{11m}\left[a^* + \theta_{1m}\sin(\gamma_m\eta)\right]\sin(m\pi\xi)$$
$$+ \sum_{m^*+1}^{\infty} G_{1m}\theta_{22m}\left[a^* + \theta_{2m}\sinh(\gamma_m\eta)\right]\sin(m\pi\xi), \tag{4}$$

where

$$a^* = \sinh(\beta_m\eta),$$

and G_{1m} is the Fourier coefficient, $m = 1, 2, ..., m^*$. The first sum is related to condition $\lambda^2 > (m\pi)^2$, the second sum ought to be used if $\lambda^2 < (m\pi)^2$, and

$$\theta_{1m} = \frac{\left[\beta_m^2 - \nu\psi^2(m\pi)^2\right]\sinh(\beta_m)}{\left[\gamma_m^2 + \nu\psi^2(m\pi)^2\right]\sin(\gamma_m)},$$
$$\theta_{2m} = -\frac{\left[\beta_m^2 - \nu\psi^2(m\pi)^2\right]\sinh(\beta_m)}{\left[\gamma_m^2 - \nu\psi^2(m\pi)^2\right]\sinh(\gamma_m)}, \tag{5}$$

$$\theta_{11m} = \frac{1}{\sinh(\beta_m) + \theta_{1m}\sin(\gamma_m)},$$
$$\theta_{22m} = \frac{1}{\sinh(\beta_m) + \theta_{1m}\sin(\gamma_m)}, \tag{6}$$

$$\beta_m = \psi\sqrt{\lambda^2 + (m\pi)^2},$$
$$\gamma_m = \psi\sqrt{\lambda^2 - (m\pi)^2} \quad \text{or} \quad \gamma_m = \psi\sqrt{(m\pi)^2 - \lambda^2}. \tag{7}$$

The solution for the BB2 is obtained from Eq. (4) by replacing G_{1m} by G_{2m} and where

$$\theta_{1m} = -\frac{\sinh(\beta_m)}{\sin(\gamma_m)},$$
$$\theta_{11m} = \frac{1}{\theta_{1m}\gamma_m^2\sin(\gamma_m) - \beta_m^2\sinh(\beta_m)}, \tag{8}$$

$$\theta_{2m} = -\frac{\sinh(\beta_m)}{\sinh(\gamma_m)},$$
$$\theta_{22m} = \frac{1}{\theta_{2m}\gamma_m^2\sinh(\gamma_m) - \beta_m^2\sinh(\beta_m)}. \tag{9}$$

The last step is to enforce the simply supported boundary condition along the hypotenuse. For this purpose, the BB1 and BB2 are overlapped. Hence, the SS-BC on two perpendicular sides of the triangle are satisfied. However, the boundary condition along the hypotenuse is enforced by adjusting the Fourier coefficients in $w_{\mathrm{BB1}}(\xi,\eta)$ and $w_{\mathrm{BB2}}(\xi,\eta)$, i.e., G_{1m} and G_{2m}. Thus along the hypotenuse, η may be written as $\eta = 1 - \xi$ and $w_{\mathrm{BB1}}(\xi, 1-\xi)$, $w_{\mathrm{BB2}}(\xi, 1-\xi)$ are obtained. Formulating the contributions of the BB1 and BB2 and adjusting the G_{1m} and G_{2m} to satisfy the bending moment along the hypotenuse, the formal solution of the problem is obtained. To solve the triangular plate free vibration problem, all boundary conditions should be simultaneously satisfied. The method leads to the system of homogeneous algebraic equations. The determinant of the coefficient matrix is equal to zero and eigenvalues λ^2 are calculated. It leads to the solution of the triangular plate free vibration problem SS-BC in the form:

$$w(\xi,\eta) = w_{\mathrm{BB1}}(\xi,\eta) + w_{\mathrm{BB2}}(\xi,\eta). \tag{10}$$

To verify the numerical code, the eigenvalues λ^2 for the first five mode shapes are calculated, and they are the same as in (Saliba, 1990). To obtain the plate deflection in the (x,y) coordinates, in the above formulas the (ξ,η) dimensionless coordinates have to be transformed again.

2.2. Determination of the a-PZT and its action on the plate

Standard (regular) piezoelectric actuators have square, rectangular and circular shapes. In a 2D analysis of the actuator acting on a plate, it is assumed that the actuator induces a bending moment along its

edge. If the piezoelectric material has the same properties in two directions, the induced bending moments are the same at each end of the cross-section of the actuator (Fuller *et al.*, 1997; Her, Chen, 2020). More precisely, in the case of a square or rectangular actuator, the bending moments at opposite edges are the same. However, in the case of a circular actuator, the bending moment along the edge is the same. As shown in (Brański, Szela, 2008; 2010), bending moments in one cross-section can be replaced by two the same pairs of forces.

To form the a-PZT, the active fibers are considered, arranged radially at a certain point on the plate. Next, it is necessary to find this point that would connect all fibers, i.e., the point around which the actuator would be created. It turns out that at this point, marked by $x_a = (x_a, y_a)$, the bending moment of the plate reaches the absolute extreme. Then, the maximum bending moment criterion is used to find the x_a (it is a common point for all fibers, and the basic one of a-PZT).

To create the shape of the a-PZT, by analogy to one-dimensional structure, namely, to the beam (Brański, Kuras, 2022), the plate bending moments in all directions with $\Delta\varphi_k = \varphi_k - \varphi_{k-1} = 1$ degree interval are calculated (Fig. 3). On separate fibers in both directions from point x_a, the points $x_k = (x_{1k}, y_{1k})$ with the same plate bending moments are found. Then the neighboring points at the ends of the fibers were connected with a line and this line created the edge of the a-PZT.

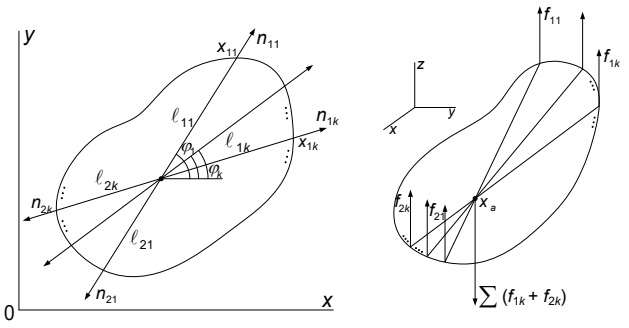

Fig. 3. The idea of constructing the a-PZT and global symbols.

An arbitrary fiber of the a-PZT acts on the plate with the bending moments:

$$2M_k = M_{1k} + M_{2k} = f_{1k}\ell_{1k} + f_{2k}\ell_{2k}, \tag{11}$$

where $\ell_k = \{\ell_{1k}, \ell_{2k}\}$ are the arm lengths of the asymmetric fiber.

Bending moments can be replaced by two pairs of forces:

$$\begin{aligned} f_{Pk} &= f_{Pk}(x,y) = f_{1k}\delta(x - x_{1k}, y - y_{1k}) \\ &\quad - (f_{1k} + f_{2k})\delta(x - x_a, y - y_a) \\ &\quad + f_{2k}\delta(x - x_{2k}, y - y_{2k}), \end{aligned} \tag{12}$$

where k – the number of PZT fibres in the actuator, $f_k = \{f_{1k}, f_{2k}\}$ – the forces due to a fibre, $\{x_{1k} = (x_{1;k}, y_{1;k}), x_a = (x_a, y_a), x_{2k} = (x_{2;k}, y_{2;k})\}$ – the points of applying forces of a fibre; for simplicity $x_k = (x_{1k}, x_{2k})$, $x = (x, y) = (r_a + r) = (r_a\cos\alpha + r\cos\varphi, r_a\sin\alpha + r\sin\varphi)$ – an arbitrary point of the plate.

Equation (12) defines the acting of one fiber of the a-PZT on a plate. To determine the acting of the a-PZT, it is necessary to sum the acting of all fibers:

$$f_P = f_P(x,y) = \sum_k f_{Pk}(x,y). \tag{13}$$

3. Forced vibration reduction by actuator

As we assumed the response of the plate and the excitation are harmonic, one can express these functions as

$$w_f(x,y) = \sum_n A_n w_n(x,y), \tag{14}$$

$$f(x,y) = \sum_n B_n w_n(x,y), \tag{15}$$

where A_n is the constant to be determined, and

$$\begin{aligned} B_n &= \frac{1}{\zeta_n}\iint_\Omega f(x,y)w_n(x,y)\,\mathrm{d}x\,\mathrm{d}y, \\ \zeta_n &= \iint_\Omega w_n^2(x,y)\,\mathrm{d}x\,\mathrm{d}y. \end{aligned} \tag{16}$$

The force $f(x,y)$ represents both the exciting force and forces due to PZT, Eq. (1), so the integral in Eq. (16) can be written as $I_n = I_{n;E} + I_{n;P}$, where

$$\begin{aligned} I_{n;E} &= \iint_\Omega f_E w_n(x,y)\,\mathrm{d}x\,\mathrm{d}y \\ &= \iint_\Omega f_0\delta(x - x_0, y - y_0)w_n(x,y)\,\mathrm{d}x\,\mathrm{d}y \\ &= f_0 w_n(x_0, y_0). \end{aligned} \tag{17}$$

According to Eq. (12)

$$\begin{aligned} I_{n;P} &= \iint_\Omega \sum_k f_{Pk}(x,y)w_n(x,y)\,\mathrm{d}x\,\mathrm{d}y \\ &= \sum_k [f_{1k}w_n(x_{1k}, y_{1k}) - (f_{1k} + f_{2k})w_n(x_a, y_a) \\ &\quad + f_{2k}w_n(x_{2k}, y_{2k})]. \end{aligned} \tag{18}$$

Substituting Eq. (11) into square brackets and after some calculations, one can obtain

$$\begin{aligned} &\sum_k [f_{1k}w_n(x_{1k}, y_{1k}) - (f_{1k} + f_{2k})w_n(x_a, y_a) \\ &\qquad + f_{2k}w_n(x_{2k}, y_{2k})] \\ &\quad = -\frac{1}{2D}\sum_k \ell_{1k}(\ell_{1k} + \ell_{2k})M_k(x_a, y_a), \end{aligned} \tag{19}$$

where $M_k(x_a, y_a)$ is the plate bending moment at point (x_a, y_a).

Equation (19) determines the direct relationship between transverse displacement of the plate caused by the actuator and the plate bending moment at the point (x_a, y_a). Based on Eqs. (17)–(19), the B_n can be calculated. Substituting Eqs. (14)–(15) into Eq. (1) and taking into account the mode shape functions, Eq. (10), the A_n coefficients can be expressed as follows:

$$A_n = \frac{B_n}{(n^2\pi^2 - \beta_n^2)^2 - \omega_f^2},$$

$$A_n = \frac{B_n}{(n^2\pi^2 + \gamma_n^2)^2 - \omega_f^2} \quad \text{or} \quad A_n = \frac{B_n}{(n^2\pi^2 - \gamma_n^2)^2 - \omega_f^2} \tag{20}$$

whichever is real.

Substituting Eq. (20) into Eq. (14):

$$w_f(x,y) = \sum_n \frac{1/\zeta\,(I_{n;E} + I_{n;P})}{(n^2\pi^2 - \beta_n^2)^2 - \omega_f^2} w_n(x,y), \tag{21}$$

and considering only the part due to excitation, one can obtain a function that is an optimization objective function:

$$I_{n;f} = f_0 w_n(x_0, y_0) - \frac{1}{2D} \sum_k \ell_{1k}\,(\ell_{1k} + \ell_{2k})\, M_k(x_a, y_a)$$
$$= I_{n;E} + I_{n;P}. \tag{22}$$

Equation (22) was used to model three types of PZT: square, circular, and asymmetrical. The $I_{n;f}$ reduction leads to a reduction of the plate vibrations. Equation (22) means that a total reduction of vibration is possible if the plate response to the exciting force f_E equals the plate response to the forces from all fibers composing the two-dimensional actuator, i.e., if $I_{n;f} = 0$. Thus, the objective function is trivial; the derived expression is minimized and can be written as follows:

$$J = \min\left(I_{n;f}\right). \tag{23}$$

4. Reduction effectiveness coefficient

The vibration reduction effectiveness is measured by analysing the vibration amplitude of the plate. The coefficient which is used to calculate the amount of vibration reduction is formulated as follows:

$$R_n = \frac{w_{n;E} - w_{n;f}}{w_{n;E}} \cdot 100\%, \tag{24}$$

where $w_{n;E}$ is the transverse displacement of the plate at the point of maximum amplitude (without PZT); vibrations are forced only by the force $f_E(x,y)$, $w_{n;f}$ – the transverse displacement of the plate at the point of maximum amplitude (with acting PZT); vibrations are forced by $f_E(x,y)$ and reduced by forces from the PZT fibers.

Similarly to R_n, other coefficients can be formulated, based, for example, on the bending moment or the shear force. The paper presents the results of R_n, because the amplitude value is related to the values of the other two quantities.

5. Analytical calculations

The object of the calculations is an isosceles right triangular plate with simply supported edges. The following data were assumed in the calculations: $a = 1$ m, $b = 1$ m, $h = 1.59 \cdot 10^{-3}$ m, $E = 71.7 \cdot 10^9$ Pa, $\varrho = 7169$ kg$\cdot$m^{-3}, $\nu = 0.33$, the lengths of each PZT fiber are the same and equal $0.2a$. The number of fibers was constant for all cases and equal 40. The amplitude of the exciting force was selected experimentally to obtain significant plate deflections for a given mode shape: $\{f_{0;n}\} = \{f_{0;1}, f_{0;2}, f_{0;3}, f_{0;4}, f_{0;5}\} = \{2, 20, 20, 40, 40\}$ N.

5.1. Vibration reduction of triangular plate via PZTs

Based on the assumptions made, the shapes of asymmetrical piezoelectric actuators are determined, and then the effect obtained after their application is compared with the effect of regular PZTs. Taking into account the asymmetric actuator determined by the exact method, its simplified version is presented, in which the asymmetry points of each fiber are arbitrarily set at the point of the maximum bending moment of the plate (Fig. 4). The quantitative results of the calculations are shown in Table 1 and Fig. 5.

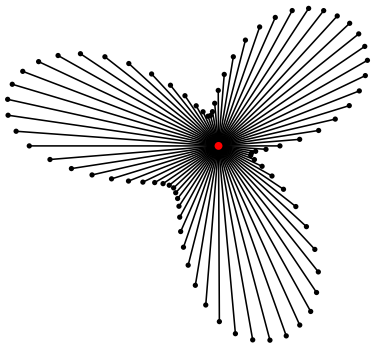

Fig. 4. a-PZT for first mode shape.

Table 1. Vibration reduction coefficient results.

Mode	R_n [%]		
	s-PZT	c-PZT	a-PZT
1	97.43	97.70	99.69
2	97.84	97.82	99.71
3	98.45	99.55	99.89
4	99.93	99.60	99.94
5	97.00	97.98	99.66

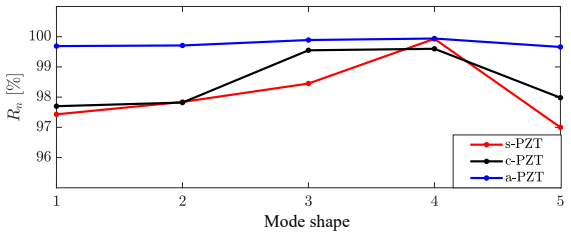

Fig. 5. R_n coefficient for first five mode shapes.

Figure 6 shows the effect of applying s-PZT, c-PZT, and a-PZT. Figures 7a–c corresponds to the first mode shape and they are compared with different shapes of actuators. Figures 7d–f shows the same for the second mode shape. In Fig. 8 there are a-PZTs for higher mode shapes.

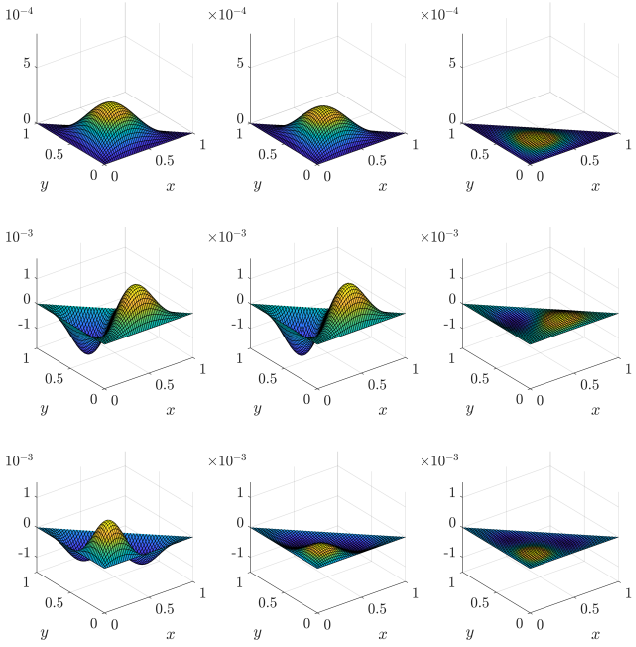

Fig. 6. Results of the PZTs acting for the first three mode shapes: s-PZT (left); c-PZT (center); a-PZT (right).

The results show a big advantage of the a-PZT over the s-PZT. The maximum difference in efficiency occurs for the 5th mode and it is almost 3%. The shape of the a-PZT closely corresponds to the shape of the nodal lines for a given mode. For the 1st, 2nd, and 5th mode shape, in which the nodal lines form triangles similar to the shape of the plate, one gets an irregular shape of the actuator with three vertexes. Moreover, for these mode shapes, a clear axial symmetry can be seen in the shape of the actuator. The axial symmetry can also be seen in the other two vibration modes, 3rd and 4th. In these cases the nodal lines in the area of the a-PZT location are close to a square with rounded vertices (one rounded vertex in the case of 3rd mode, Fig. 8a, two rounded vertices in the case

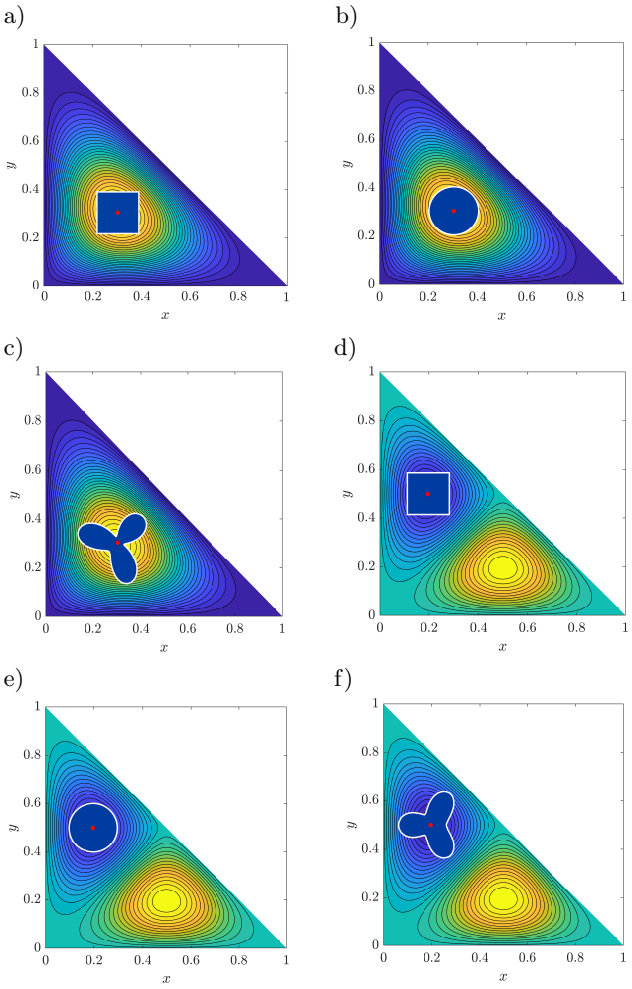

Fig. 7. PZTs shapes and locations for the first two mode shapes – 1st mode shape: a) s-PZT, b) c-PZT, c) a-PZT; 2nd mode shape: d) s-PZT, e) c-PZT, f) a-PZT.

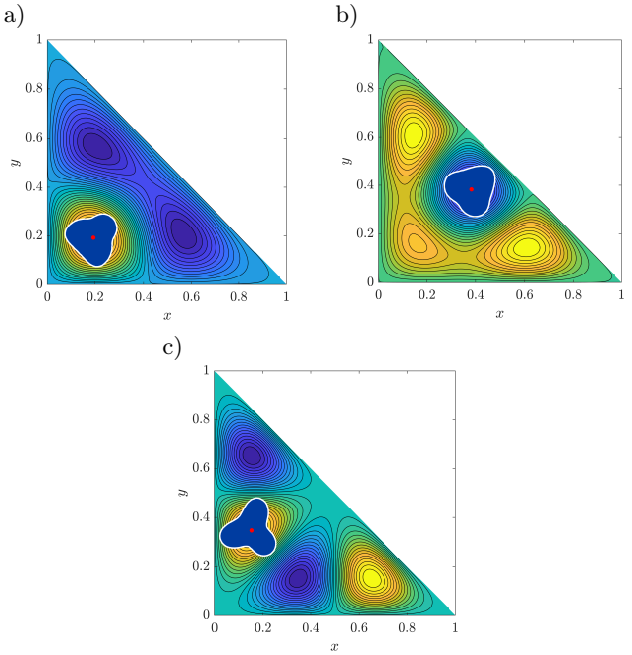

Fig. 8. a-PZTs shapes and locations for other mode shapes: a) 3rd mode shape; b) 4th mode shape; c) 5th mode shape.

of 4th mode, Fig. 8b). In these cases the axial symmetry is due to the plate geometry (isosceles triangle).

The shape of the nodal lines also affects the difference between the efficiency of the c-PZT and the a-PZT. It can be seen that for 1st, 2nd, and 5th mode shapes the difference is about 2% in favour of the a-PZT. However, for 3rd, 4th, and higher mode shapes, the reduction effectiveness coefficient for the c-PZT is very close to the a-PZT. The greater difference in efficiency for these mode shapes can be seen with the reduction of the PZT fiber length.

6. Conclusions

The article presents an active vibration reduction of triangular plate via asymmetrical PZT. Based on the principle of operation of the PZT, the problem of its optimal shape was solved. This led to the creation of the a-PZT. It consists of radial one-dimensional fiber actuators with a common point. This point is located at the maximum plate bending moment. Each actuator fiber was considered separately to optimize its arm lengths. By joining the adjacent ends of the separate fibers, an a-PZT shape was created. The a-PZT provides the most effective reduction of vibrations for a given structure. The results, presented in Table 1, show that the use of the a-PZT in the active reduction of vibrations of two-dimensional structures provides greater efficiency than regular actuators, both square and circular ones. Based on the calculations, the conclusions can be formulated:

- the a-PZT consists of the radial one-dimensional fiber actuators with a common point;
- this is the basic a-PZT point at which the plate bending moment reaches its maximum; it leads to the formulation of the maximum bending moment criterion, to obtain the a-PZT shape;
- the a-PZT reduces vibration more effectively than s-PZT and c-PZT assuming the same energy added to all systems;
- the a-PZT shape closely correlates with the nodal lines of a given mode, i.e., the type of asymmetry depends on the shape of the nodal lines around the maximum plate bending moment.

The idea of the a-PZT presented in the paper can be a starting point for considerations on the active reduction of vibrations of more complex two-dimensional structures, e.g., cylindrical or three-dimensional structures.

Acknowledgments

This research did not receive any specific grant from funding agencies in the public, commercial, or not-for-profit sectors.

Declaration of conflicting interests

The Authors declare that there is no conflict of interest.

References

1. Aridogan A., Basdogan I. (2015), A review of active vibration and noise suppression of plate-like structures with piezoelectric transducers, *Journal of Intelligent Material Systems and Structures*, **26**(12): 1455–1476, doi: 10.1177/1045389X15585896.
2. Brański A., Szela S. (2008), Improvement of effectiveness in active triangular plate vibration reduction, *Archives of Acoustics*, **33**(4): 521–530.
3. Brański A., Szela S. (2010), Quasi-optimal PZT distribution in active vibration reduction of the triangular plate with P-F-F boundary conditions, *Archives of Control Sciences*, **20**(2): 209–226, doi: 10.2478/v10170-010-0014-7.
4. Brański A., Kuras R. (2022), Asymmetrical PZT applied to active reduction of asymmetrically vibrating beam – semi-analytical solution, *Archives of Acoustics*, **47**(4): 555–564, doi: 10.24425/aoa.2022.142891.
5. Donoso A., Sigmund O. (2009), Optimization of piezoelectric bimorph actuators with active damping for static and dynamic loads, *Structural and Multidisciplinary Optimization*, **38**: 171–183, doi: 10.1007/s00158-008-0273-0.
6. Fuller C.R., Elliot S.J., Nielsen P.A. (1997), *Active Control of Vibration*, Academic Press, London.
7. Gardonio P., Casagrande D. (2017), Shunted piezoelectric patch vibration absorber on two-dimensional thin structures: Tuning considerations, *Journal of Sound and Vibration*, **395**: 26–47, doi: 10.1016/j.jsv.2017.02.019.
8. Gonçalves J.F., De Leon D.M., Perondi E.A. (2017), Topology optimization of embedded piezoelectric actuators considering control spillover effects, *Journal of Sound and Vibration*, **388**: 20–41, doi: 10.1016/j.jsv.2016.11.001.
9. Gorman D.J. (1983), A highly accurate analytical solution for free vibration analysis of simply supported right triangular plates, *Journal of Sound and Vibration*, **89**(1): 107–118, doi: 10.1016/0022-460X(83)90914-8.
10. Gorman D.J. (1999), *Vibration analysis of Plates by the Superposition Method*, World Scientific Publishing Co. Pte. Ltd., Singapore.
11. Hansen C.H., Snyder S.D. (1997), *Active Control of Noise and Vibration*, E & FN SPON, London.
12. Her S.-C., Chen H.-Y. (2020), Deformation of composite laminates induced by surface bonded and embedded piezoelectric actuators, *Materials*, **13**(14): 3201, doi: 10.3390/ma13143201.

13. Kozień M.S., Ścisło Ł. (2015), Simulation of control algorithm for active reduction of transversal vibrations of beams by piezoelectric elements based on identification of bending moment, *Acta Physica Polonica A*, **128**(1): A56–A61, doi: 10.12693/APhysPolA.128.A-56.

14. Leissa A.W. (1969), *Vibration of Plates*, Scientific and Technical Information Division NASA, Washington.

15. Rao S.S. (2007), *Vibration of Continuous Systems*, John Wiley & Sons Inc., Hoboken, New Jersey.

16. Saliba H.T. (1990), Transverse free vibration of simply supported right triangular thin plates: A highly accurate simplified solution, *Journal of Sound and Vibration*, **139**(2): 289–297, doi: 10.1016/0022-460X(90)90889-8.

17. Saliba H.T. (1996), Free vibration of simply supported general triangular thin plates: An accurate simplified solution, *Journal of Sound and Vibration*, **196**(1): 45–57, doi: 10.1006/jsvi.1996.0466.

18. Sun Y., Song Z., Li F. (2022), Theoretical and experimental studies of an effective active vibration control method based on the deflection shape theory and optimal algorithm, *Mechanical Systems and Signal Processing*, **170**: 108650, doi: 10.1016/j.ymssp.2021.108650.

19. Trojanowski R., Wiciak J. (2020), Impact of the size of the sensor part on sensor-actuator efficiency, *Journal of Theoretical and Applied Mechanics*, **58**(2): 391–401, doi: 10.15632/jtam-pl/118948.

20. Wang W. (2003), *Electrode shape optimization of piezoelectric transducers*, Ph.D. Thesis, University of Florida.

21. Zhang X., Takezawa A., Kang Z. (2018), Topology optimization of piezoelectric smart structures for minimum energy consumption under active control, *Structural and Multidisciplinary Optimization*, **58**: 185–199, doi: 10.1007/s00158-017-1886-y.

22. Zorić N.D., Tomović A.M., Obradović A.M., Radulović R.D., Petrović G.R. (2019), Active vibration control of smart composite plates using optimized self-tuning fuzzy logic controller with optimization of placement, sizing and orientation of PFRC actuators, *Journal of Sound and Vibration*, **456**: 173–198, doi: 10.1016/j.jsv.2019.05.035.